Pure

Scotland's Rural College

A high-throughput analysis of high-resolution X-ray CT images of stems of olive and citrus plants resistant and susceptible to Xylella fastidiosa

Walker, Nancy C.; Ruiz, Siul A.; Ferreira, Talita R.; Coletta-Filho, Helvecio D.; Le Houx, James; McKay Fletcher, Daniel; White, Steven M.; Roose, Tiina

Published in:
Plant Pathology

DOI:
10.1111/ppa.13835

First published: 27/11/2023

Document Version
Publisher's PDF, also known as Version of record

Link to publication

Download date: 09. Jan. 2024

ORIGINAL ARTICLE

Plant Pathology An International Journal edited by the British Society for Plant Pathology

WILEY

A high-throughput analysis of high-resolution X-ray CT images of stems of olive and citrus plants resistant and susceptible to *Xylella fastidiosa*

Nancy C. Walker[1] [ID] | Siul A. Ruiz[1] | Talita R. Ferreira[2] | Helvecio D. Coletta-Filho[3] [ID] |
James Le Houx[4] | Daniel McKay Fletcher[5] | Steven M. White[6] [ID] | Tiina Roose[1] [ID]

[1]Bioengineering Sciences Research Group, Department of Mechanical Engineering, School of Engineering, Faculty of Engineering and Physical Sciences, University of Southampton, Southampton, UK

[2]Brazilian Synchrotron Light Laboratory (LNLS), Brazilian Center for Research in Energy and Materials (CNPEM), Campinas, Brazil

[3]Instituto Agronômico de Campinas, Centro de Citricultura Sylvio Moreira, Cordeirópolis, Brazil

[4]Diamond Light Source, Harwell Campus, Didcot, UK

[5]Rural Economy Environment and Society Research Group, SRUC, Edinburgh, UK

[6]UK Centre for Ecology & Hydrology, Maclean Building, Crowmarsh Gifford, UK

Correspondence
Tiina Roose, Bioengineering Sciences Research Group, Department of Mechanical Engineering, School of Engineering, Faculty of Engineering and Physical Sciences, University of Southampton, Southampton SO17 1BJ, UK.
Email: t.roose@soton.ac.uk

Funding information
NERC, Grant/Award Number: NE/S00720/1

Abstract

The bacterial plant pathogen *Xylella fastidiosa* causes disease in several globally important crops. However, some cultivars harbour reduced bacterial loads and express few symptoms. Evidence considering plant species in isolation suggests xylem structure influences cultivar susceptibility to *X. fastidiosa*. We test this theory more broadly by analysing high-resolution synchrotron X-ray computed tomography of healthy and infected plant vasculature from two taxonomic groups containing susceptible and resistant varieties: two citrus cultivars (sweet orange cv. Pera, tangor cv. Murcott) and two olive cultivars (Koroneiki, Leccino). Results found the susceptible plants had more vessels than resistant ones, which could promote within-host pathogen spread. However, features associated with resistance were not shared by citrus and olive. While xylem vessels in resistant citrus stems had comparable diameters to those in susceptible plants, resistant olives had narrower vessels that could limit biofilm spread. And while differences among olive cultivars were not detected, results suggest greater vascular connectivity in resistant compared to susceptible citrus plants. We hypothesize that this provides alternate flow paths for sustaining hydraulic functionality under infection. In summary, this work elucidates different physiological resistance mechanisms between two taxonomic groups, while supporting the existence of an intertaxonomical metric that could speed up the identification of candidate-resistant plants.

KEYWORDS
citrus variegated chlorosis, olive quick decline syndrome, resistance, X-ray computed tomography, *Xylella fastidiosa*, xylem

1 | INTRODUCTION

The plant pathogen *Xylella fastidiosa* (Wells et al., 1987) is a major threat to plant health worldwide (Almeida et al., 2019), colonizing over 600 plant species (Delbianco et al., 2022). In South America, many diseases associated with *X. fastidiosa* are attributed to subspecies *pauca*, its only native subspecies. In 1987, a devastating disease outbreak occurred in Brazilian citrus trees, which

was later associated with this bacterium (Chang et al., 1993; Lee et al., 1991). Since then, citrus variegated chlorosis (CVC) has been responsible for the removal of more than 100 million citrus trees in Brazil (Bové & Ayres, 2007). Despite the devastation caused, the severity of the disease led to significant research advances that informed the development of a successful management programme to mitigate disease spread (Coletta-Filho et al., 2020). As a result, CVC in Brazil is now largely under control, with 1.7% of sweet orange plants being infected with *X. fastidiosa* in 2019 (Coletta-Filho et al., 2020) compared with 43.8% in 2004 (EFSA Panel on Plant Health et al., 2018). Despite the success in reducing instances of CVC, *X. fastidiosa* is still prevalent in the Brazilian environment and continues to present an agricultural threat. Recently, *X. fastidiosa* subsp. *pauca* has been found infecting olive plants sampled in Brazil showing desiccation symptoms (Coletta-Filho et al., 2016). This disease of olive, the olive quick decline syndrome (OQDS), is not just a local concern. In Italy, a recent OQDS outbreak represents the first known introduction of *X. fastidiosa* into Europe (Saponari, Giampetruzzi, et al., 2019). Since that introduction, more than 21 million olive trees across southern Italy have died, and predicted losses could reach €5.2 billion by 2050 (Schneider et al., 2020). Because no cure to CVC or OQDS is known to date (Bragard et al., 2019a), there is an urgent need for effective and sustainable control strategies to limit further damage.

Although *X. fastidiosa* causes severe disease, there can be significant variation in response to infection, even among genetically similar hosts (Amanifar & Luvisi, 2022; Boscia et al., 2017; de Souza et al., 2009; Krivanek & Walker, 2005; Ledbetter & Rogers, 2009). Some varieties of a particular taxonomic group may be highly susceptible, with high pathogen populations and severe symptoms, while others, termed resistant, exhibit low bacterial counts and limited symptoms (Agrios, 2005). Studies have shown the possibility of mitigating the impact of *X. fastidiosa* by replanting susceptible plants with resistant varieties (Bragard et al., 2019b). As well as maintaining crop yield, given *X. fastidiosa* acquisition efficiency is correlated with bacterial load (Hill & Purcell, 1997), resistant plants also have the potential to limit epidemiological spread. Within the genus *Citrus*, sweet orange (*C. sinensis*) varieties are the most susceptible to *X. fastidiosa*; analysis of a germplasm collection containing about 200 accessions of sweet orange did not detect any resistant genotypes (Laranjeira et al., 1998). However, various genotypes of mandarin (*C. reticulata*), lemon (*C. limon*) and tangor (*C. sinensis* × *C. reticulata*), among others, are considered resistant, testing negative for *X. fastidiosa* under high disease pressure (Laranjeira et al., 1998). Though many traditional Italian olive (*Olea europea*) cultivars are susceptible, two resistant cultivars, Leccino and FS17 (or Favolosa), have been confirmed (Boscia et al., 2017; Giampetruzzi et al., 2016; Luvisi et al., 2017). Present opinion suggests that these cultivars will be critical to rebuilding lost agriculture in Italy (Pavan et al., 2021; Saponari, Altamura, et al., 2019). However, despite the fact that resistant plant varieties have been identified, traits and mechanisms facilitating their preferential response to pathogen invasion are poorly understood.

A number of biochemical traits have been correlated with *X. fastidiosa* resistance. These include aspects of xylem composition, for example lignin has been associated with the resistance of olive cv. Leccino (Sabella et al., 2018), and genetic factors, for example Rodrigues et al. (2013) report the induction of several genes in infected resistant Ponkan mandarin, hypothesized to play a role in its defence response. Xylem physiology is also hypothesized to contribute to differential responses to *X. fastidiosa* infection (Carluccio et al., 2023). As such, aspects of xylem structure in resistant and susceptible plants have been measured and compared.

A recent study compared xylary pit structure in olive cultivars Cellina di Nardò and Leccino (Montilon et al., 2022). Xylary pits, that is, xylem vessel wall perforations spanned by a thin, porous membrane, function to allow water to flow between vessels while preventing the spread of dangerous air embolisms and invading pathogens. It was found that pit membranes within infected plants of susceptible olive cultivar Cellina di Nardò had a degraded appearance. In contrast, in infected Leccino plants, pit membranes remained intact and impermeable to the bacteria. Another study considered pit structure in sweet orange cv. Pera, highly susceptible to CVC, and the resistant Murcott tangor (Niza et al., 2015). Niza et al. (2015) hypothesized that the small pits found in vessels of the secondary xylem across both varieties could contribute to the generally slow bacterial migration in citrus. However, differences in pit structure between the cultivars were not found. In general, due to their size, investigation into differential pitting and its role in disease resistance has been limited. In particular, though pit structure has been somewhat investigated, studies have not yet examined differences in abundance and distribution of xylary pits (Carluccio et al., 2023). A greater abundance of pits could provide critical hydraulic flow paths, acting to promote pathogen and air-embolism spread through degraded pit membranes, or, if pit membranes remain intact, facilitating routes to bypass vessel occlusions. As such, increased vascular connectivity could act to promote either resistance or susceptibility to *X. fastidiosa*. One study made quantitative estimates of vascular connectivity in stems of susceptible and resistant grapevines by counting vessel relays—radial chains of short, narrow conducting elements connecting larger diameter vessels (Brodersen et al., 2013). More vessel relays were found within stems of the susceptible cultivar, suggesting that among grapevines, vascular connectivity acts to exacerbate disease symptoms. We hypothesize that differences in the number of intervessel connections probably represents an important differential trend among many susceptible versus resistant plants and should be further investigated.

Xylem vessels are much wider than their pits and thus can be measured using less sophisticated imaging techniques. Consequently, there is growing literature concerning the relevance of xylem vessel diameters to *X. fastidiosa* disease resistance (Chatelet et al., 2011; Coletta-Filho et al., 2007; Sabella et al., 2019; Walker et al., 2022). Narrower vessels have slower flow rates. Furthermore, because there is a linear relationship between the diameter of a xylem vessel and that of its largest pit (Martínez-Vilalta et al., 2002), it is expected

TABLE 1 Infection methods and plant health status determination.

Plant	No. of scanned replicates	Method of infection	Length of infection	Confirmed by PCR of leaf tissue?	Symptoms
Citrus cv. Pera (susceptible)	6 infected/6 healthy	Pin prick	>3 years	Yes	Irregular leaves chlorosis
Citrus cv. Murcott (resistant)	6 infected/6 healthy	Pin prick	1 month (no colonization)	No (no colonization)	None
Olive cv. Koroneiki (susceptible)	3 infected/4 healthy	Naturally infected	Unknown	Yes	Desiccated leaves
Olive cv. Leccino (resistant)	4 infected/4 healthy	Naturally infected	Unknown	Yes	None

that narrow vessels should have smaller pits. As such, though not explicitly demonstrated, it is hypothesized that narrow vessels act to limit the spread of both pathogen- and stress-induced embolisms (Petit et al., 2021; Walker et al., 2022). It is consistently reported that resistant olive cv. Leccino has narrower vessels than susceptible olive cultivars (Sabella et al., 2019; Walker et al., 2022). However, one study found that vessels in stems of resistant olive cv. FS17 had diameters comparable to those in susceptible cultivars (Walker et al., 2022). Furthermore, in citrus, varying levels of *X. fastidiosa* susceptibility demonstrated among sweet orange cv. Pera and tangor cv. Murcott hybrids could not be correlated with xylem vessel diameters (Coletta-Filho et al., 2007). As such, further investigation into the generality of the reported trend in Leccino is needed.

Previous studies considering the influence of xylem physiology on *X. fastidiosa* resistance only consider a limited number of closely related plant species (Carluccio et al., 2023). Most *X. fastidiosa* subspecies and sequence types (STs) do not cause disease in plants susceptible to other *X. fastidiosa* subspecies and STs, and as such, it is expected that they should interact differently in their respective hosts. However, although providing useful information, framing our studies this way makes it difficult to make generalizations. Furthermore, most studies only consider healthy plants. Only one study has compared vessel lumen sizes across healthy and infected plants resistant (olive cv. Leccino) and susceptible (olive cv. Cellina di Nardò) to *X. fastidiosa* (Sabella et al., 2020). Though no differences were found in vessel lumen sizes (width or area) between vessels in healthy and infected stems of each cultivar, authors found significantly more vessel occlusions in infected stems of susceptible compared to resistant plants. Though beyond the scope of xylem anatomy, this study demonstrated that comparing images of infected and healthy stems could provide important information regarding the contribution of stem vascular occlusions to disease severity. Finally, many of the aforementioned studies were limited in the measurements that could be made due to the two-dimensional nature of the imaging technique. The study of Walker et al. (2022) was one of the first to employ 3D X-ray computed tomography (XCT) to this scope, enabling the quantification of many more vessels per sample in a consistent automated manner. Beyond providing a platform for processing these large quantities of data, Walker et al. (2022) linked

physiological features to fluid mechanical processes, for example hydraulic conductivity and embolism resistance, which are essential for sustaining transpiration rates. However, this study was also limited, both in the number of samples and types of features that could be analysed, due to the resolution limits and time-consuming nature of benchtop XCT.

Synchrotron X-ray computed tomography (SXRCT) has the capability to image internal structures much faster, and at higher resolution, than comparative benchtop methods. In this study, using state-of-the-art 3D SXRCT, we assess the xylem vasculature in healthy and infected stems from one susceptible and one resistant variety of plant species grown in Brazil belonging to two *Citrus* species (sweet orange cv. Pera and tangor cv. Murcott) and two olive cultivars (Koroneiki and Leccino). Using two different methods, we measured vessel diameters, also allowing us to make inferences regarding infection-induced vessel occlusions, and made quantitative estimates of intervessel connectivity. Furthermore, using fluid mechanical models, we investigated whether mechanisms can be inferred by which measured anatomical traits could be influencing the susceptibility of the considered plant species/cultivars.

2 | MATERIALS AND METHODS

2.1 | Choice of plants

We studied plants from two *Citrus* species: one susceptible to *X. fastidiosa* infection, *C. sinensis* 'Pera', and one resistant, tangor, *C. sinensis × C. reticulata* 'Murcott', a hybrid of mandarin and sweet orange. We also considered one susceptible and one resistant olive cultivar, cv. Koroneiki and cv. Leccino. Citrus samples were taken from plants grown in greenhouse conditions, while olive samples were taken from plants in the natural environment in an area with high inoculum pressure (22°18′58.8″ S, 45°22′28.1″ W). Both healthy and infected plants were used in this study. The citrus plants were inoculated with *X. fastidiosa* strain 9a5c at 10^8–10^9 cfu/mL. All plants were tested for the presence of *X. fastidiosa* using real-time quantitative PCR (Oliveira et al., 2002). Details of infection methods and health status determination are given in Table 1.
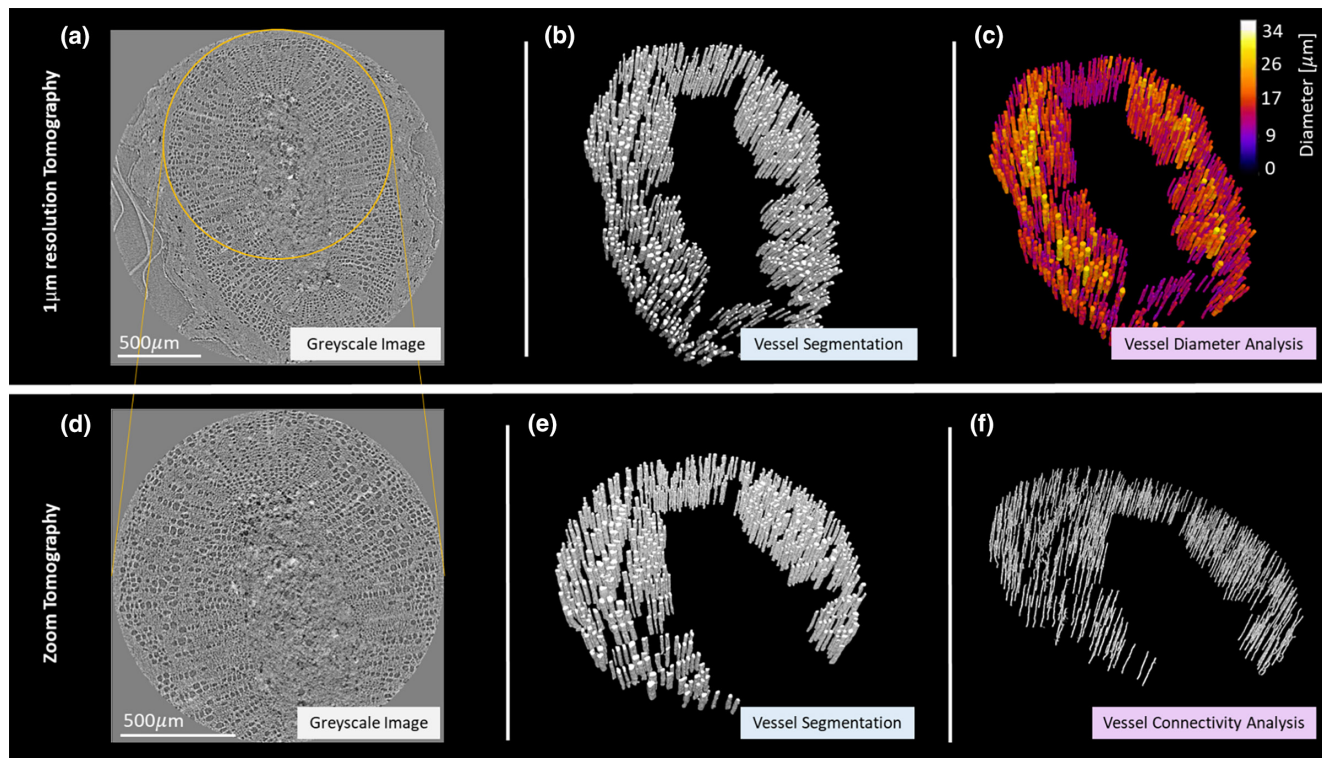
FIGURE 1 All stem samples (39 stems) were scanned at 1 μm resolution (a). For one stem of each type (eight stems, e.g. as shown; olive, healthy, susceptible), a zoomed image was acquired at 685 nm resolution (d). The field of view for the zoom was chosen to optimize the volume of xylem tissue contained within the image. Both 1 μm resolution and zoom images were processed and analysed. First, the greyscale images (a,d) were segmented (b,e) following the protocol outlined by Walker et al. (2022). Then, thickness maps (c) were generated from the 1 μm resolution images, from which vessel diameter measurements could be extracted. Skeletons (f) were generated from the zoom images, from which inferences pertaining to vascular connectivity could be drawn.[Colour figure can be viewed at wileyonlinelibrary.com]

2.2 | Sample selection and preparation

We sampled stems from three trees of each plant species/cultivar and sanitary status. Infected plants were sampled just below visible symptoms, and healthy plants at comparable locations, that is, of similar (c. 2 mm) diameter. All samples were dried in a desiccator for 2 weeks to ensure xylem vessels were void of water, maximizing contrast-to-noise ratio. As described by Walker et al. (2022), we assume shrinking of vessel pores due to drying to be linear across all samples, and thus comparisons between measurements to be representative. Replicating the set up described by Walker et al. (2022), samples were mounted inside narrow carbon fibre tubing, held tightly by a cling film wrap. This was to minimize lateral sample movement during scanning that could introduce unwanted image noise.

2.3 | XCT scanning

Two samples were scanned from each citrus plant and one from each olive plant, with six citrus and three olive replicates from each cultivar and health status. An additional sample from one plant of each of healthy Leccino, infected Leccino and healthy Koroneiki were also scanned. Numbers of scanned replicates are given explicitly in Table 1.

SXRCT was conducted at the MOGNO beamline of the Brazilian synchrotron light source (Sirius) (Archilha et al., 2022). Projection data were acquired under quasi-monochromatic beam conditions (22 ± 1.4 keV), enabled by a set of multilayer mirrors, with a 0.5 μm Si filter to eliminate photon energies <10 keV. We used a 2048×2048 pixels sCMOS-based detector with a 5× objective lens. All samples were scanned using source-to-object and source-to-detector distances of 704 mm and 964 mm, respectively, achieving an effective pixel size of 998 nm (Figure 1a).

One sample of each plant type and each health status was scanned again over a smaller region at higher resolution. Images obtained under these settings are denoted 'zoom images' (Figure 1d). Zoom images were achieved by reducing the source-to-object distance to 484 mm, resulting in an estimated pixel size of 685 nm. For all scans, 2048 projections were collected over 360° rotation using a 0.6 s exposure time. A single closed-beam and open-beam reference image was taken for flat- and dark-field corrections. The average scan time for both settings was approximately 20 min. All images were reconstructed using an in-house implementation of the FDK algorithm (Miqueles et al., 2020) for cone-beam tomographic data (available upon request). The implementation is based on a multi-GPU approach taking about 40 s to perform Radon inversion in floating-point precision of a measured dataset of $2048 \times 2048 \times 2048$ voxels.

WILEY | 5

2.4 | Image segmentation

We adapted the previously established image segmentation framework outlined in Walker et al. (2022). All modifications to the methodology were made on the basis of image quality.

Prior to segmentation, image filtering and enhancement was carried out to remove artefacts and enhance xylem features. First, a 3D isometric (4 voxel radius) median filter was applied to filter out speckle noise. Then, a 3D isometric (4 voxel radius) mean filter was applied to smooth out the data. Finally, a 3D anisometric ellipsoidal (axes of 2, 2 and 10 voxels) mean filter was applied, based on the elongated shape of the xylem vessels along the depth (z-direction). This had the purpose of enhancing xylem vessel features while suppressing noise or other irrelevant objects in the images.

Due to the filtering, the grey-value histogram of resulting image stacks was unimodal. Thus, image segmentation was achieved using the ImageJ default threshold; a variation of the IsoData algorithm (Ridler & Calvard, 1978). Unlike Otsu (1979), this algorithm is not based on the modality of the histogram. It works by first taking a sufficiently low initial threshold, then computing the mean grey value of voxels above and below the threshold, respectively. The mean of these two averages then defines a new threshold. This process is repeated until the new threshold is larger than the next composite average, having the effect of defining two grey-value classes (corresponding to tissue and pore) with minimal within-class variability.

Additional post-processing was required due to image noise associated with the synchrotron images. A number of erosions were applied to segmented image stacks. To ensure we did not remove features of interest, we limited the relative erosion to be no more than half the size of the smallest considered vessel diameter measured by Walker et al. (2022). On this basis, three erosions were applied across all thresholded images, and one extra erosion across each thresholded zoom image. 'Fill holes' and 'watershed' binary processes were applied across all images as described by Walker et al. (2022). These binary processes were applied after the first two erosions to minimize the potential of creating new artefacts, while retaining important features.

Connected component labelling was carried out on the resulting 'segmented stack', creating a 32-bit 'labelled stack'. The top and bottom slice in each labelled stack was imported into a Python script which checked which labels were present in both slices. Corresponding vessels were designated 'spanning'. The collection of all spanning vessels was used for subsequent analysis based on the methodology of Walker et al. (2022).

2.5 | Assessment of xylem vessel diameters

Segmented stacks of just spanning vessels were re-dilated, generating a 'dilated span stack' (Figure 1b). This was to ensure that before applying the BoneJ Thickness function (Doube et al., 2010) to generate the 'thickness stack' (Figure 1c), the spanning vessels were true to size, regardless of labelling approach. Labelled and thickness stacks were used to obtain diameter measurements as described by Walker et al. (2022).

2.6 | Assessment of xylem connectivity

We were unable to explicitly quantify intervessel pits in our images. From literature, these features are approximately 0.5–1.5 μm in size (Niza et al., 2015). As such, it is expected that they should be beyond our resolution limit, which we deem to be approximately 5× estimated pixel size. Instead, we estimate the connectivity of segmented vascular networks by considering the proximity of isolated vessels. As a first estimate, we consider the proportion of spanning vessels in direct contact. To do this, we first generated a new labelled stack based on the dilated span stack, that is, the stack in which the spanning vessels are true to size. The number of labelled connected components was then compared with the original labelled stack to infer how many vessels are connected. We then segmented the zoom images as described above (Figure 1e) and used those to generate skeletons (Figure 1f) via the BONEJ toolbox (Doube et al., 2010). The number of connected groups of spanning vessels (skeletons), the length of all branches in each skeleton, and the angle of orientation of each branch was quantified. Within each skeleton, we assume a branch >5 μm in length and >30° to the most vertical branch to be indicative of a vessel connection, either to another spanning vessel or to some other conducting element. This branch filtering was to ensure that we excluded branches corresponding to the spanning vessels themselves and to minimize any contributions that could be coming from skeletonization artefacts. Analysis was done on the raw numbers of these branches. Despite not having all the information to determine true xylem connectivity, we gauge this metric as a proxy, interpreting these branches as possible neighbouring conduit connections acting to either promote pathogen spread or deviate flow around infected zones.

2.7 | Statistics

All statistics were carried out using the Scipy Python library (Virtanen et al., 2020). Considered vessel diameters correspond to the mean of measurements at every 1 μm depth. Statistics were applied on the mean vessel diameter for each scan (i.e., each scan is a statistical replicate). We applied a two-tailed Student's t test to assess differences between the mean diameters pertaining to resistant versus susceptible and healthy versus infected citrus and olive stems. For connectivity analysis, the means of all groups were compared using Tukey's honestly significant difference (HSD). All statistical tests were applied with a significance threshold of $p < 0.05$, and all reported p-values are given to three decimal places.

We also considered vessel size distributions corresponding to groups between which significant differences were found comparing the mean diameter. Presented distributions are given in terms of the probability density function (pdf), where bin heights are equal to the empirical probability of a measurement landing in that bin, divided by the bin width. In contrast, distributions considered to make theoretical inferences used raw histograms, where bin heights correspond to the relative frequencies that measurements land in the corresponding bins. All distributions considered all spanning vessels from all stems of the relevant sample type. All distributions were given sufficiently few bins to ensure that the bin width was greater than the image estimated pixel size.

2.8 | Applied mathematical models

2.8.1 | Hydraulic conductivity

Following Walker et al. (2022), we invoke the Hagen-–Poiseuille relation to model hydraulic flow rates through segmented vessels. The volumetric flow rate through all vessels from all stems of a given plant type and health status (Q_{tot}) of diameters up to a given value (d [m]) is given by

$$Q_{\text{tot}}(d) = \frac{\pi}{128\eta} \sum_{d_i < d} d_i^4 \cdot \left(-\frac{\Delta p}{\Delta z} \right),\tag{1}$$

where d_i [m] are the bin edges of the defining size histogram, η [Pas] is water viscosity and Δp [Pa] is the pressure drop along the vessel section of length Δz [m]. We assume parameter values $\eta = 10^{-3}$ [Pas], the viscosity of water, $\Delta z = 1.8 \times 10^{-3}$ [m], the length of the considered vessel sections and $\Delta p = -0.1 \times 10^{-6}$ [Pa]. The value of Δp was chosen for consistency with Walker et al. (2022).

Modelled volumetric flow rate through a representative stem of the given sample type and health status (Q [m^3 s^{-1}]) is given by

$$Q = \frac{1}{N_{\text{stem}}} Q_{\text{tot}}(d_{\text{max}}),\tag{2}$$

where N_{stem} [–] is the total number of such stems and d_{max} [m], the largest diameter considering all vessels from all stems.

2.8.2 | Mathematical model of biofilm spread in xylem vessels

In order to model pathogen spread in segmented vessels, we employ a model (File S1) that describes the interaction between growing biofilm and xylem sap flow within an isolated infected vessel in a transpiring tree. Under the assumption that biofilm structure is dominated by the physics of extracellular polymeric substance (EPS) molecules, this model approximates *X. fastidiosa* biofilm as a polymer gel, while xylem sap is approximated as pure water. Model simulations were run in two dimensions, with the vessel geometry approximated as a rectangle. The height of

the theoretical vessel was varied according to diameter measurements extracted from our SXRCT images. The length of the theoretical vessel was fixed, representing a control vessel sub-length. Under the assumption that the infection level should be similar throughout the vessel length, a periodic condition was prescribed at the inlet and outlet. Transpiration was modelled using a diurnal pressure condition applied consistently across all simulations. Model simulations were computed for 100 days, and total flux of water and biofilm across the vessel outlet calculated. An important mechanism of the model considers the potential for biofilm to block a vessel. Once a vessel becomes fully occluded, subsequent biofilm and water transport is halted.

We consider 19 vessel diameters at evenly spaced intervals between 9.62 and 28.6 µm. Integrating the volume of biofilm through each modelled vessel with the averaged vessel size distribution from all healthy stems of each plant type, we obtain a predicted cumulative spread of biofilm (V_{tot} [m^3]) through vessels of sizes up to a given diameter d [m]. The integral was calculated discretely as:

$$V_{\text{tot}}(d) = \sum_{d_j < d} \widetilde{V}_b(d_j) \cdot \overline{H}(d_j),\tag{3}$$

where d_j [m] are diameters for which simulations were run, $\overline{H}$ [–] is the histogram of vessels sizes for the given plant type with bin edges defined by the d_j, and $\widetilde{V}_b$ [m^3] is the volume of biofilm moved through the model vessel of diameter d_j.

An estimate for the volume of biofilm through a representative stem of each plant type (V [m^3]) is therefore given as

$$V(d) = \frac{1}{N_{\text{stem}}} V_{\text{tot}}(d_{\text{max}}).\tag{4}$$

3 | RESULTS

3.1 | Vessel diameter statistics

A *t* test was applied between mean vessel diameters in stems of healthy and infected citrus (Table 2a) and olive (Table 2b) cultivars. The two important significant results come from comparing values from healthy and infected susceptible olive stems and from susceptible and resistant healthy olive stems.

3.2 | Loss of hydraulic functionality in infected versus healthy susceptible olives

There was a significant difference comparing mean diameters of vessels from infected versus healthy susceptible olive stems. The corresponding size distributions highlight that the infected stems had on average smaller vessels and also relatively fewer large vessels (Figure 2a). Using the Hagen–Poiseuille relation (Equation 1), we infer that this corresponds to a greater drop in the average volumetric flow through the stem compared with the other plant types (Equation 2; Figure 2b,c).

TABLE 2 Comparing mean vessel diameters in healthy and infected stems of citrus (a) and olive cultivars (b).

Pairwise *t*-tests	Healthy susceptible	Infected susceptible	Healthy resistant	Infected resistant
(a)				
Healthy susceptible	$\mu = 17.7$ $\sigma = 1.40$	$p = 0.099$	$p = 0.333$	$p = 0.615$
Infected susceptible		$\mu = 19.4$ $\sigma = 1.42$	$p = 0.845$	$p = 0.294$
Healthy resistant			$\mu = 19.1$ $\sigma = 2.68$	$p = 0.561$
Infected resistant				$\mu = 18.2$ $\sigma = 1.77$
(b)				
Healthy susceptible	$\mu = 16.4$ $\sigma = 0.771$	$p < 0.05^*$	$p < 0.05^*$	$p < 0.05^*$
Infected susceptible		$\mu = 14.5$ $\sigma = 0.537$	$p = 0.776$	$p = 0.423$
Healthy resistant			$\mu = 14.3$ $\sigma = 0.996$	$p = 0.577$
Infected resistant				$\mu = 13.8$ $\sigma = 1.16$

Note: Table diagonals show mean (μ) and standard deviation (σ) of all diameter measurements from all vessels across all scans of the given plant type and health status. Significant differences are denoted by *. Measurements associated with the significant results highlighted in dark shading are examined in greater detail. The result in light shading can be considered to follow from those in dark shading.

3.3 | Reduced biofilm spread in resistant versus susceptible olives

We measured vessel diameter distributions (Figure 3a) as well as inferring cumulative biofilm spread using a developed mathematical model (Figure 3b). There was a significant difference comparing mean diameters of vessels from healthy susceptible versus resistant olive stems (Table 2). Full diameter distributions illustrate that the resistant cultivar had both on average smaller vessels and showed absence of the widest vessels (Figure 3a). Integrating the volume of biofilm moving through modelled vessels over 100 days with the vessel size distributions of healthy resistant and susceptible citrus and olive stems (Equation 3), we present a predicted relative cumulative spread of biofilm through vessels of different diameter in the vasculature of each plant variety (Equation 4; Figure 3b).

3.4 | Assessment of connections between spanning vessels

In both citrus and olives, stems from the susceptible plants had more spanning vessels than the resistant ones (Figure 4a). Estimating the proportion of spanning vessels in contact in each scan (Figure 4b) followed by a Tukey's HSD test illustrated that there was no statistical difference among the olive cultivars ($p = 1.000$) or between the susceptible citrus and susceptible and resistant olive cultivars ($p = 0.818$ and $p = 0.839$, respectively). However, there was a significant difference comparing the resistant citrus cultivar with all other plant types ($p < 0.05$, Tukey's HSD).

3.5 | Network connectivity using zoom tomography

In the skeletonized zoom images, spanning vessels were either isolated (Figure 5a), branching (Figure 5b) or connected to each other (Figure 5c). The average number of branch connections per vessel (Figure 5d) was not significantly different comparing susceptible and resistant olive stems ($p = 0.899$, Tukey's HSD). However, we did find significant differences comparing all other groups ($p < 0.05$, Tukey's HSD), in particular, resistant versus susceptible citrus stems.

4 | DISCUSSION

X. fastidiosa is a plant pathogen of increasing global concern (Almeida et al., 2019; Castro et al., 2021). Resistant plants are considered a critical resource for rebuilding lost agriculture (Saponari, Altamura, et al., 2019); however, traits facilitating their preferential response to infection remain poorly characterized. Here, we scanned healthy and infected stems of resistant and susceptible citrus and olive cultivars with 3D SXRCT at two different resolutions. In doing so, we were able to attain a much richer dataset than has been considered previously, allowing us to make more extensive inferences, and with greater statistical weighting.

Two scans were excluded from all analyses on the basis that the corresponding samples were much wider than the others, and thus deemed to be outliers (File S2). From the remaining images, we isolated 'spanning vessels', defined as those spanning the full stem
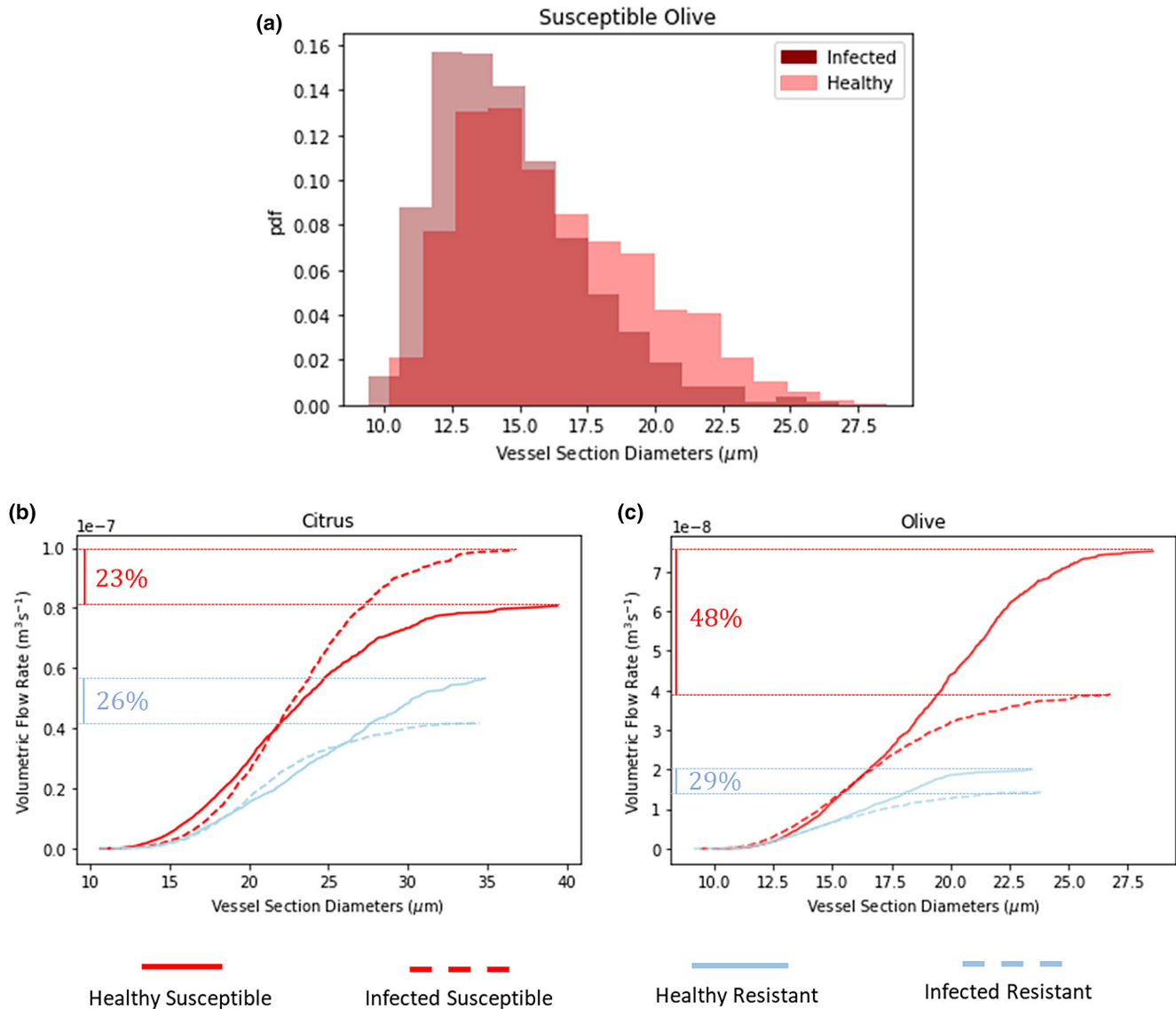
FIGURE 2 Histograms showing the distribution of vessel diameters across all replicates of infected and healthy susceptible olives (a), together with estimates of volumetric flow rates through representative healthy and infected citrus (b) and olive (c) stems. Hydraulic estimates are based on the Poiseuille flow solution (Equation 2), considering the cumulative contribution from vessels of increasing diameter across all stems. The total flow rate through a representative healthy compared to infected susceptible olive stem corresponds to a 48% drop-off in conductivity, compared with 29% in resistant olives, and 26% and 23% in resistant and susceptible citrus, respectively.[Colour figure can be viewed at wileyonlinelibrary.com]

sample length, using an automated method (Walker et al., 2022). In general, xylem vessel length is positively correlated with diameter (Hacke et al., 2006; Sperry et al., 2005), and wider vessels are more conductive (Zimmermann, 2013). As such, spanning vessels can be considered to be the most important to hydraulic function, particularly under healthy conditions (Equation 1).

One physiological metric often discussed in relation to *X. fastidiosa* resistance is xylem vessel diameter. We compared the average vessel diameter in stems of healthy and infected, resistant and susceptible plants of both citrus and olive. While differences were found comparing average vessel diameters in the healthy susceptible olive stems with those from all other olive groups, we found no significant differences between resistant and susceptible healthy and

infected citrus varieties. Finding differences comparing vessel diameters in plants of olive cv. Leccino compared with those in susceptible olive cultivars is consistent with a relatively extensive literature (Sabella et al., 2019; Walker et al., 2022). Furthermore, Coletta-Filho et al. (2007) found no correlation between vessel diameters and the relative susceptibility and resistance among infected hybrids of sweet orange cv. Pera and tangor cv. Murcott. Here, we provide further evidence that xylem vessel diameters do not immediately play a role in the susceptibility, or resistance, of citrus plants.

Results showed significant differences in the mean vessel diameter measured in infected compared to healthy susceptible olive stems. The work of Cardinale et al. (2018) suggests vessel occlusion to be important to disease symptoms in susceptible olive

FIGURE 3 Histograms of vessel diameters across all replicates of healthy susceptible and resistant olives (a), together with model estimates of mean biofilm spread in the vasculature of all citrus and olive varieties (b).[Colour figure can be viewed at wileyonlinelibrary.com]
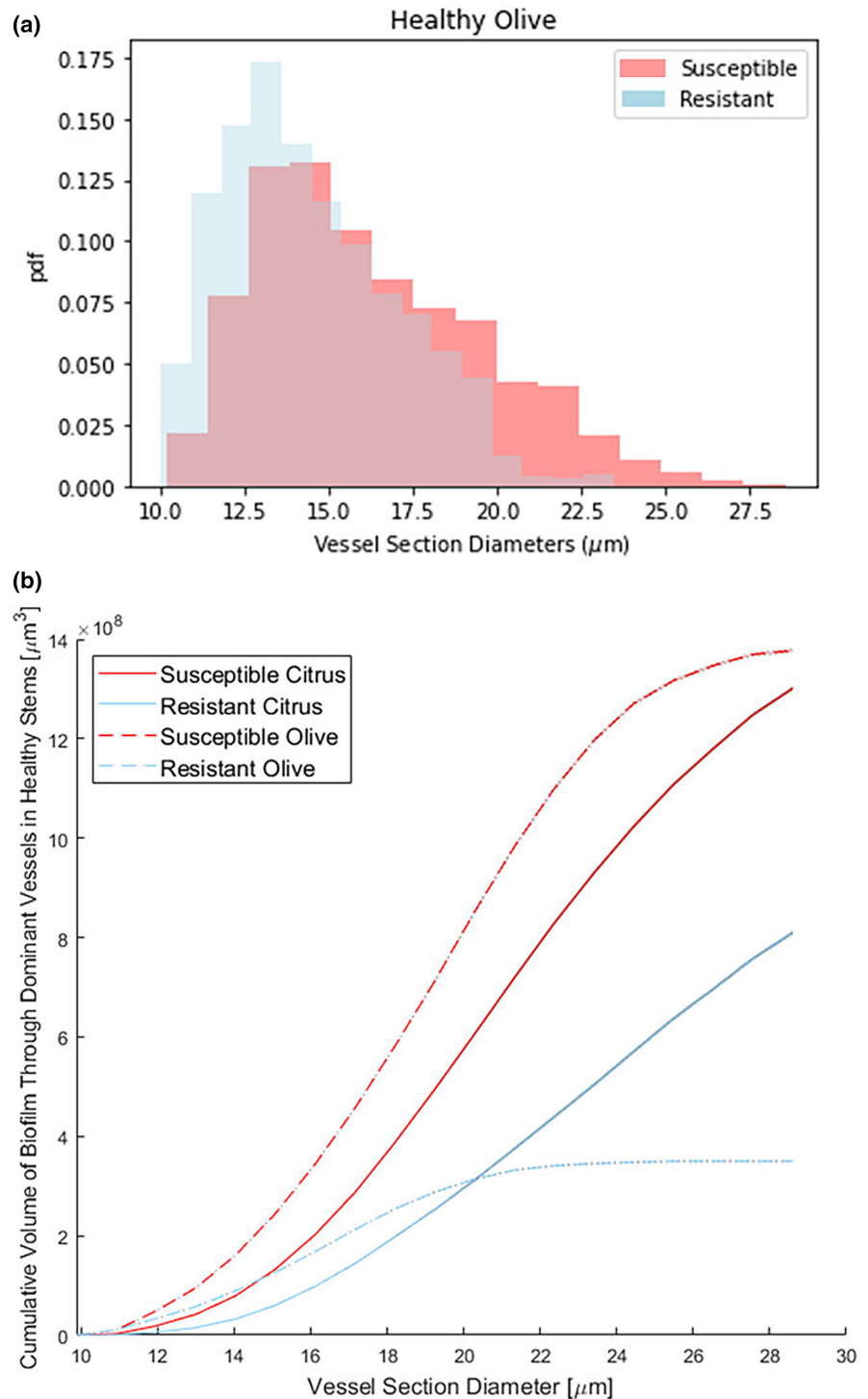
cultivar Ogliarola Salentina. Though beyond the capabilities of the presented data, we can speculate that the drop-off in the proportion of the largest measured vessel diameters between healthy and infected susceptible olives is a result of vessel occlusions. Using the Hagen–Poiseuille relation (Equation 1), we could extend our inferences to the impact of these occlusions on vascular functionality by estimating the volumetric flow through healthy compared to infected plant stems of each variety (Equation 2). Hagen–Poiseuille illustrates that the narrow vessels in resistant

olive cv. Leccino result in slower flow rates than in the other plant stems. Similarly transforming diameter measurements using Hagen–Poiseuille, both Petit et al. (2021) and Walker et al. (2022) showed that Leccino stems are consistently less conductive than those from susceptible olive cultivars. However, the results of the present study also highlight a comparatively large drop-off in hydraulic flow through the healthy versus infected susceptible olive stems (48%) compared with the other plant varieties (20%–30%). Using theoretical inferences pertaining to air embolisms, Walker
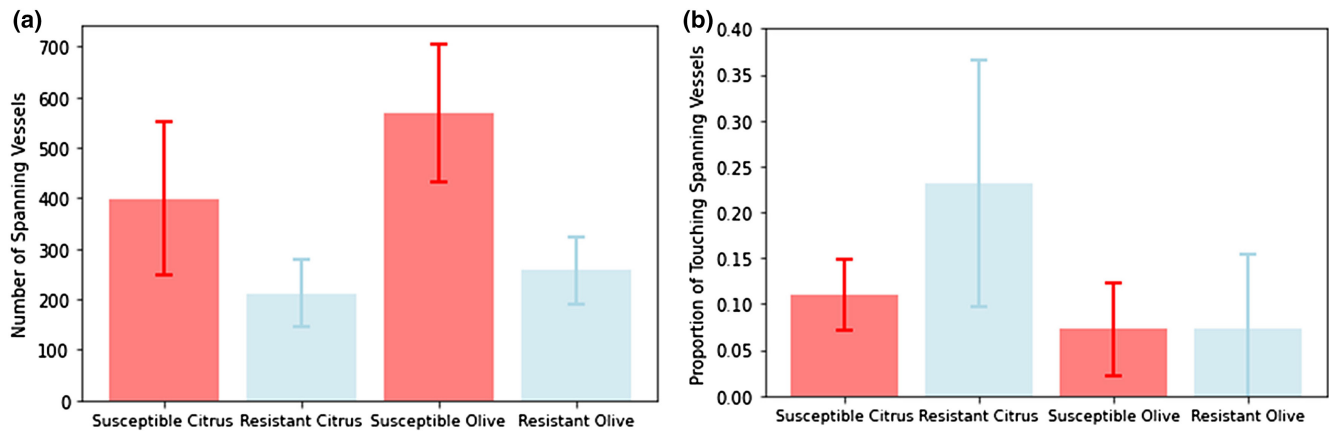
FIGURE 4 Bar plots representing the number of spanning vessels (a) and proportion of spanning vessels in contact (b) within 1 μm resolution images. The height of each bar corresponds to the mean value considering healthy and infected stems of the given plant type. Error bars represent standard deviation.[Colour figure can be viewed at wileyonlinelibrary.com]
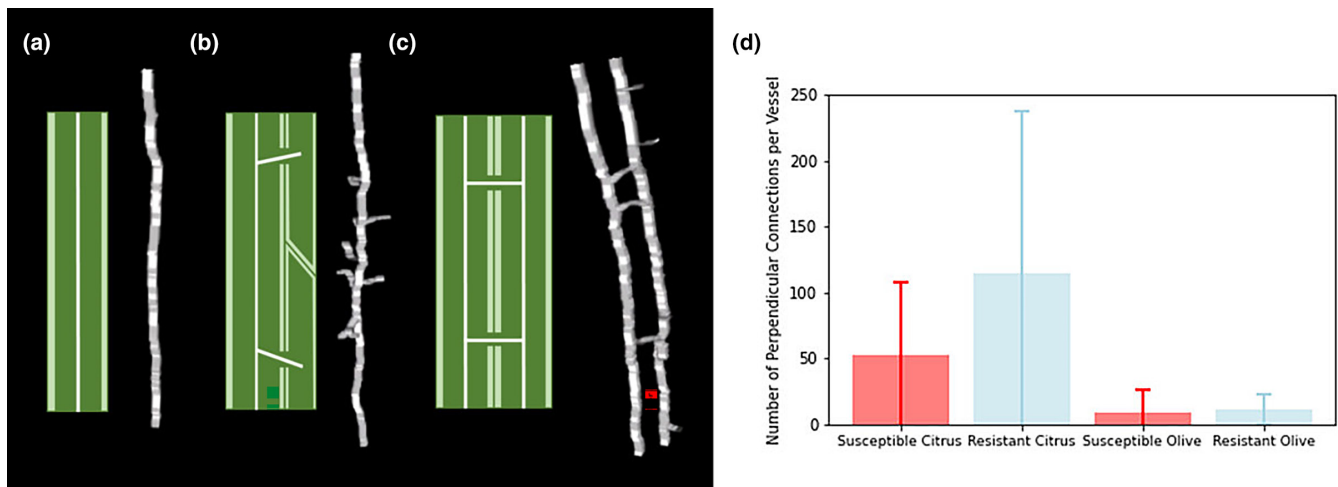

FIGURE 5 Visual representation of types of connectivity demonstrated by skeletonization: (a) isolated, (b) branching and (c) connected, and a bar plot (d) representing the number of inferred connections per vessel in the zoom images. The height of each bar corresponds to the mean value considering healthy and infected stems of the given plant type. Error bars represent standard deviation.[Colour figure can be viewed at wileyonlinelibrary.com]

et al. (2022) show that the increased susceptibility of larger vessels to air embolism could lead to a significant reduction in hydraulic functionality, exacerbating disease symptoms. The result of the present study complements the previous result, showing that this phenomenon is not just a threat posed by the possibility of air embolisms, but rather, occurs as a result of infection-induced occlusions.

Our diameter measurements also showed significant differences between healthy resistant and susceptible olives. Using a similar segmentation and analysis approach, Walker et al. (2022) found no significant differences comparing vessel diameters from replicates of resistant and susceptible olive cultivars. However, this was probably due to having limited replicates, with authors reporting significant differences when treating each vessel as a pseudo-replicate. Qualitatively, the distribution of vessel sizes in resistant compared to susceptible olive cultivars align with those presented by Walker

et al. (2022), as well as other studies comparing vessel diameters in Leccino and Cellina di Nardò (Petit et al., 2021; Sabella et al., 2019). Using these distributions, and those corresponding to the considered citrus plants, we were able to extend these inferences by use of a mathematical model of biofilm development and spread in xylem vessels. The results estimate reduced spread in the vasculature of both resistant plant types, but particularly in that of resistant olive cv. Leccino. This difference can be attributed to the faster flow and late biofilm bridging in the widest vessels which were not measured in Leccino plants. We hypothesize that, due to the size of the differences in predicted spread estimates, narrow vessels limiting pathogen motility acts as a primary mechanism facilitating the resistance of Leccino.

It is understood that *X. fastidiosa* moves between xylem vessels through intervessel pits (Chatterjee et al., 2008; Montilon et al., 2022; Pérez-Donoso et al., 2010; Roper et al., 2007). A number

of authors suggest aspects pertaining to the connectivity of the vasculature could be important in dictating the plant's response to *X. fastidiosa* infection (Chatelet et al., 2011; Ingel et al., 2019; Montilon et al., 2022; Sun et al., 2011). Previous studies have analysed pit structure in relation to *X. fastidiosa* disease resistance (Montilon et al., 2022; Niza et al., 2015); however, studies have not yet examined differences in the distributions of these pits, which could equally have significant implications for pathogen virulence. One study made estimates of vascular connectivity by counting vessel relays (Brodersen et al., 2013). In the present study, we estimate vascular connectivity by counting direct vessel contacts, inferring that pit connections would exist on those surfaces. Our results show that the resistant citrus variety had significantly more spanning vessels in direct contact than the susceptible variety, while there were no significant differences between the considered olive cultivars. Instances of high connectivity among spanning vessels could be indicative of critical flow paths facilitating sustained hydraulic functionality under infection. Though Brodersen et al. (2013) found the opposite trend in grapevines, we hypothesize that higher vascular connectivity is instead a favourable trait in infected citrus and acts as a resistance mechanism in plants of tangor cv. Murcott.

To provide further evidence to support this hypothesis, we made use of high-resolution zoom tomography; using segmented vessel branching to infer connections between pairs of spanning vessels, as well as to other neighbouring conducting elements. Again, results suggest higher intervessel connectivity among spanning vessels in the resistant compared to susceptible citrus plants, while finding no significant differences between resistant and susceptible olives. We note that the stems of citrus genotypes have mostly pitted element vessels, which have the smallest pit membranes, and the vessels are almost fully coated with lignin (Alves et al., 2009; Niza et al., 2015). In contrast, in grapevine stems the secondary cell wall is mainly composed of scalariform element vessels (Sun et al., 2006) which are much more permissive to the bacteria. Furthermore, in CVC-resistant genotypes, the bacteria are unable to colonize the vasculature, remaining close to the inoculation point (Niza et al., 2015). In susceptible genotypes, though colonization is progressive over time, it remains slow (Niza et al., 2015). In olive, significant long-range bacterial dispersal is observed in stems of both resistant and susceptible cultivars (dos Santos et al., 2022). We hypothesize the localized *X. fastidiosa* colonies in citrus plants would form larger, more robust bacterial aggregates, increasing the significance of alternative flow paths to sustain transpiration. However, we acknowledge that further evidence is needed to give these inferences robustness. First, we only considered one zoom image from each plant type and each health status. This was on the basis of beamtime limitations and prioritizing the standard resolution tomography. Secondly, we only considered segmented spanning vessels due to the fact that with current resolution limits, these were the only xylem features we could be confident about. As such, we could not examine the influence of smaller conducting features or count pit pores. We opted to use the MOGNO μCT beamline in order to explore the flexibility of monitoring xylary features at multiple scales. Though this is in its preliminary stages, the beamline shows promise for better understanding these multiscale processes. Furthermore, we wanted to compare infected and healthy plant material, which was readily available in Brazil as there were no regulations regarding spread of *X. fastidiosa*. However, we acknowledge that there is another 3D X-ray imaging technique, based on coherent X-rays, which can generate ptychographic nanotomography, capable of achieving much higher spatial resolution (c. 30 nm) than is possible via the direct μCT employed here. However, due to the indirect nature of the acquisition, this technique is significantly slower than the direct method. As a consequence, it is usually used to image very small samples (typically O [10 μm] in diameter), and overall throughput is much more restricted. Future advancements in SXRCT will provide imaging capabilities that will enable quantification of finer features, for example pits, while retaining high sample throughput. Future studies could make use of this technology to examine this hypothesized trait in citrus in more detail and with a greater number of samples.

Our results show that, in both citrus and olives, the susceptible plants had significantly more spanning vessels than the resistant ones. We hypothesize that this is due to the fact that such vessels, being the longest and widest conductive features, would act to promote long-range pathogen spread within plant vasculature. Importantly, this result could suggest a more general trait that could play a role across a number of hosts. Assessing the number of spanning vessels in a short stem section could provide a relatively simple way of identifying resistant or susceptible plants. Our results suggest that plants in which approximately 2-mm-diameter stems contain less than 300 spanning vessels over a depth of 1.8 mm could be candidate-resistant varieties, warranting further testing. We suggest more plant varieties are assessed to support and extend the relevance of this observation.

In summary, we examined healthy and infected vasculature of plants resistant and susceptible to *X. fastidiosa* across taxa using state-of-the-art SXRCT. We found in both citrus and olive, susceptible plant varieties had a greater number of spanning vessels. Physiological host traits have previously only been correlated with *X. fastidiosa* susceptibility on an individual taxonomic basis. Here, we elucidate a more general trait that could be of particular importance for classifying resistant and susceptible plants, particularly in the inevitable instance of future novel disease outbreaks. Results pertaining to both methods of pathogenicity and possible resistance mechanisms found differences among citrus and olives. We detected significant stem occlusions in susceptible olives, but not in the other plants, suggesting that stem occlusion is a primary method of pathogenicity in olive, but not citrus. Furthermore, we found the resistant olive cultivar to have much narrower vessels than the other plants. With evidence from mathematical model simulations, we hypothesize these vessels act to mitigate pathogen spread within the host. Finally, we were able to make novel inferences regarding vascular connectivity; a metric that has not been assessed previously within this context. Results suggest stem connectivity may play an important role in the resistance of citrus varieties, but not in olive. Overall, these results show that while many physiological factors

differentiating within-host infection dynamics are pathosystem-dependent, more broad-reaching traits can be demonstrated. Resistant plants pose the most important means for rebuilding lost agriculture. The traits identified in this study will be of significant importance to future screening protocols that aim to differentiate between susceptible and resistant host plants.

DATA AVAILABILITY STATEMENT

All reconstructed 8-bit image stacks and scripts for processing and analysis are openly available from the University of Southampton repository at: https://doi.org/10.5258/SOTON/D2709.

ORCID

Nancy C. Walker https://orcid.org/0000-0003-2297-1046
Helvecio D. Coletta-Filho https://orcid.org/0000-0002-1382-4629
Steven M. White https://orcid.org/0000-0002-3192-9969
Tiina Roose https://orcid.org/0000-0001-8710-1063

REFERENCES

Agrios, G.N. (2005) *Plant pathology*. Amsterdam: Elsevier.

Almeida, R., De La Fuente, L., Koebnik, R., Lopes, J., Parnell, S. & Scherm, H. (2019) Addressing the new global threat of *Xylella fastidiosa*. *Phytopathology*, 109, 172–174.

Alves, E., Leite, B., Pascholati, S.F., Ishida, M.L. & Andersen, P.C. (2009) *Citrus sinensis* leaf petiole and blade colonization by *Xylella fastidiosa*: details of xylem vessel occlusion. *Scientia Agricola*, 66, 218–224.

Amanifar, N. & Luvisi, A. (2022) Resistance of almond (*Prunus dulcis*) to *Xylella fastidiosa*: a comparative study on cultivars. *Plant Disease*, 106, 2625–2630.

Archilha, N., Costa, G.R., Ferreira, G., Moreno, G.B.Z.L., Rocha, A.S., Meyer, B.C. et al. (2022) MOGNO, the nano and microtomography beamline at Sirius, the Brazilian synchrotron light source. *Proceedings of the Journal of Physics: Conference Series*, 2380, 012123.

Boscia, D., Altamura, G., Ciniero, A., Di Carolo, M., Dongiovanni, C., Fumarola, G. et al. (2017) Resistenza a *Xylella fastidiosa* in diverse cultivar di olivo. *L'informatore Agrario*, 11, 59–63.

Bové, J.M. & Ayres, A.J. (2007) Etiology of three recent diseases of citrus in Sao Paulo state: sudden death, variegated chlorosis and huanglongbing. *IUBMB Life*, 59, 346–354.

Bragard, C., Dehnen-Schmutz, K., Di Serio, F., Gonthier, P., Jacques, M.A., Miret, J.A.J. et al. (2019a) EFSA panel on plant health: effectiveness of in planta control measures for *Xylella fastidiosa*. *EFSA Journal*, 17, e05666.

Bragard, C., Dehnen-Schmutz, K., Di Serio, F., Gonthier, P., Jacques, M.A., Miret, J.A.J. et al. (2019b) EFSA panel on plant health: update of the scientific opinion on the risks to plant health posed by *Xylella fastidiosa* in the EU territory. *EFSA Journal*, 17, e05665.

Brodersen, C.R., Choat, B., Chatelet, D.S., Shackel, K.A., Matthews, M.A. & McElrone, A.J. (2013) Xylem vessel relays contribute to radial connectivity in grapevine stems (*Vitis vinifera* and *V. arizonica*; Vitaceae). *American Journal of Botany*, 100, 314–321.

Cardinale, M., Luvisi, A., Meyer, J.B., Sabella, E., De Bellis, L., Cruz, A.C. et al. (2018) Specific fluorescence in situ hybridization (FISH) test to highlight colonization of xylem vessels by *Xylella fastidiosa* in naturally infected olive trees (*Olea europaea* L.). *Frontiers in Plant Science*, 9, 431.

Carluccio, G., Greco, D., Sabella, E., Vergine, M., De Bellis, L. & Luvisi, A. (2023) Xylem embolism and pathogens: can the vessel anatomy of woody plants contribute to *X. fastidiosa* resistance? *Pathogens*, 12, 825.

Castro, C., Disalvo, B. & Roper, M.C. (2021) *Xylella fastidiosa*: a reemerging plant pathogen that threatens crops globally. *PLoS Pathogens*, 17, e1009813.

Chang, C.J., Garnier, M., Zreik, L., Rossetti, V. & Bové, J.M. (1993) Culture and serological detection of the xylem-limited bacterium causing citrus variegated chlorosis and its identification as a strain of *Xylella fastidiosa*. *Current Microbiology*, 27, 137–142.

Chatelet, D.S., Wistrom, C.M., Purcell, A.H., Rost, T.L. & Matthews, M.A. (2011) Xylem structure of four grape varieties and 12 alternative hosts to the xylem-limited bacterium *Xylella fastidious*. *Annals of Botany*, 108, 73–85.

Chatterjee, S., Almeida, R.P.P. & Lindow, S. (2008) Living in two worlds: the plant and insect lifestyles of *Xylella fastidiosa*. *Annual Review of Phytopathology*, 46, 243–271.

Coletta-Filho, H., Pereira, E., Souza, A., Takita, M., Cristofani-Yale, M. & Machado, M. (2007) Analysis of resistance to *Xylella fastidiosa* within a hybrid population of Pera sweet orange × Murcott tangor. *Plant Pathology*, 56, 661–668.

Coletta-Filho, H.D., Castillo, A.I., Laranjeira, F.F., de Andrade, E.C., Silva, N.T., de Souza, A.A. et al. (2020) Citrus variegated chlorosis: an overview of 30 years of research and disease management. *Tropical Plant Pathology*, 45, 175–191.

Coletta-Filho, H.D., Francisco, C.S., Lopes, J.R.S., De Oliveira, A.F. & De Oliveira Da Silva, L.F. (2016) First report of olive leaf scorch in Brazil, associated with *Xylella fastidiosa* subsp. *pauca*. *Phytopathologia Mediterranea*, 55, 130–135.

de Souza, A.A., Takita, M.A., Amaral, A.D., Coletta-Filho, H. & Machado, M.A. (2009) Citrus responses to *Xylella fastidiosa* infection, the causal agent of citrus variegated chlorosis. *Tree and Forestry Science and Biotechnology*, 3, 73–80.

Delbianco, A., Gibin, D., Pasinato, L. & Morelli, M. (2022) European food safety authority: update of the *Xylella* spp. host plant database – systematic literature search up to 30 June 2021. *EFSA Journal*, 20, e07039.

dos Santos, B.D.N., Anguita-Maeso, M. & Coletta-Filho, H.D. (2022) Transmission and distribution of *Xylella fastidiosa* subsp. *pauca* in olive trees as a parameter for managing olive quick decline syndrome. *Plant Pathology*, 71, 1849–1858.

Doube, M., Kłosowski, M.M., Arganda-Carreras, I., Cordelières, F.P., Dougherty, R.P., Jackson, J.S. et al. (2010) BoneJ: free and extensible bone image analysis in ImageJ. *Bone*, 47, 1076–1079.

EFSA Panel on Plant Health, Jeger, M., Caffier, D., Candresse, T., Chatzivassiliou, E., Dehnen-Schmutz, K. et al. (2018) Updated pest categorisation of *Xylella fastidiosa*. *EFSA Journal*, 16, e05357.

Giampetruzzi, A., Morelli, M., Saponari, M., Loconsole, G., Chiumenti, M., Boscia, D. et al. (2016) Transcriptome profiling of two olive cultivars in response to infection by the CoDiRO strain of *Xylella fastidiosa* subsp. *pauca*. *BMC Genomics*, 17, 475.

Hacke, U.G., Sperry, J.S., Wheeler, J.K. & Castro, L. (2006) Scaling of angiosperm xylem structure with safety and efficiency. *Tree Physiology*, 26, 689–701.

Hill, B. & Purcell, A. (1997) Populations of *Xylella fastidiosa* in plants required for transmission by an efficient vector. *Phytopathology*, 87, 1197–1201.

Ingel, B., Jeske, D.R., Sun, Q., Grosskopf, J. & Roper, M.C. (2019) *Xylella fastidiosa* endoglucanases mediate the rate of Pierce's disease development in *Vitis vinifera* in a cultivar-dependent manner. *Molecular Plant–Microbe Interactions*, 32, 1402–1414.

Krivanek, A. & Walker, M. (2005) *Vitis* resistance to Pierce's disease is characterized by differential *Xylella fastidiosa* populations in stems and leaves. *Phytopathology*, 95, 44–52.

Laranjeira, F., Pompeu, J., Jr., Garcia, A., Jr., Vleirs, M., Harakava, R. & Beretta, M. (1998) Screening for tolerance of citrus to *Xylella fastidiosa*, the causal agent of citrus variegated chlorosis CVC. *Fruits*, 53, 345.

Ledbetter, C.A. & Rogers, E.E. (2009) Differential susceptibility of *Prunus* germplasm (subgenus *Amygdalus*) to a California isolate of *Xylella fastidiosa*. *HortScience*, 44, 1928–1931.

Lee, R., Derrick, K., Beretta, M., Chagas, C. & Rossetti, V. (1991) Citrus variegated chlorosis: a new destructive disease of citrus in Brazil. *Citrus Industry*, 72, 12–15.

Luvisi, A., Aprile, A., Sabella, E., Vergine, M., Nicolì, F., Nutricati, E. et al. (2017) *Xylella fastidiosa* subsp. *pauca* (CoDiRO strain) infection in four olive (*Olea europaea* L.) cultivars: profile of phenolic compounds in leaves and progression of leaf scorch symptoms. *Phytopathologia Mediterranea*, 56, 259–273.

Martínez-Vilalta, J., Prat, E., Oliveras, I. & Piñol, J. (2002) Xylem hydraulic properties of roots and stems of nine Mediterranean woody species. *Oecologia*, 133, 19–29.

Miqueles, E.X., Martinez, G., Jr. & Guerrero, P.P. (2020) Fast image reconstruction at a synchrotron laboratory. In: *Proceedings of the proceedings of the 2020 SIAM conference on parallel processing for scientific computing*. Philadelphia, USA: SIAM, pp. 24–34.

Montilon, V., De Stradis, A., Saponari, M., Kubaa, R.A., Giampetruzzi, A., D'Attoma, G. et al. (2022) *Xylella fastidiosa* subsp. *pauca* ST53 exploits pit membranes of susceptible olive cultivars to spread systematically in the xylem. *Plant Pathology*, 72, 144–153.

Niza, B., Coletta-Filho, H., Merfa, M., Takita, M. & de Souza, A. (2015) Differential colonization patterns of *Xylella fastidiosa* infecting citrus genotypes. *Plant Pathology*, 64, 1259–1269.

Oliveira, A.C., Vallim, M.A., Semighini, C.P., Araújo, W.L., Goldman, G.H. & Machado, M.A. (2002) Quantification of *Xylella fastidiosa* from citrus trees by real-time polymerase chain reaction assay. *Phytopathology*, 92, 1048–1054.

Otsu, N. (1979) A threshold selection method from gray-level histograms. *IEEE Transactions on Systems, Man, and Cybernetics*, 9, 62–66.

Pavan, S., Vergine, M., Nicolì, F., Sabella, E., Aprile, A., Negro, C. et al. (2021) Screening of olive biodiversity defines genotypes potentially resistant to *Xylella fastidiosa*. *Frontiers in Plant Science*, 12, 723879.

Pérez-Donoso, A.G., Sun, Q., Roper, M.C., Greve, L.C., Kirkpatrick, B. & Labavitch, J.M. (2010) Cell wall-degrading enzymes enlarge the pore size of intervessel pit membranes in healthy and *Xylella fastidiosa*-infected grapevines. *Plant Physiology*, 152, 1748–1759.

Petit, G., Bleve, G., Gallo, A., Mita, G., Montanaro, G., Nuzzo, V. et al. (2021) Susceptibility to *Xylella fastidiosa* and functional xylem anatomy in *Olea europaea*: revisiting a tale of plant–pathogen interaction. *AoB Plants*, 13, plab027.

Ridler, T. & Calvard, S. (1978) Picture thresholding using an iterative selection method. *IEEE Transactions on Systems, Man, and Cybernetics*, 8, 630–632.

Rodrigues, C.M., de Souza, A.A., Takita, M.A., Kishi, L.T. & Machado, M.A. (2013) RNA-Seq analysis of *Citrus reticulata* in the early stages of *Xylella fastidiosa* infection reveals auxin-related genes as a defense response. *BMC Genomics*, 14, 676.

Roper, M.C., Greve, L.C., Warren, J.G., Labavitch, J.M. & Kirkpatrick, B.C. (2007) *Xylella fastidiosa* requires polygalacturonase for colonization and pathogenicity in *Vitis vinifera* grapevines. *Molecular Plant–Microbe Interactions*, 20, 411–419.

Sabella, E., Aprile, A., Genga, A., Siciliano, T., Nutricati, E., Nicolì, F. et al. (2019) Xylem cavitation susceptibility and refilling mechanisms in olive trees infected by *Xylella fastidiosa*. *Scientific Reports*, 9, 9602.

Sabella, E., Luvisi, A., Aprile, A., Negro, C., Vergine, M., Nicolì, F. et al. (2018) *Xylella fastidiosa* induces differential expression of lignification related-genes and lignin accumulation in tolerant olive trees cv. Leccino. *Journal of Plant Physiology*, 220, 60–68.

Sabella, E., Moretti, S., Gärtner, H., Luvisi, A., De Bellis, L., Verine, M. et al. (2020) Increase in ring width, vessel number and δ18O in olive trees infected with *Xylella fastidiosa*. *Tree Physiology*, 40, 1583–1594.

Saponari, M., Altamura, G., Abou Kubaa, R., Montilon, V., Saldarelli, P., Specchia, F. et al. (2019) Further acquisition on the response of a large number of olive cultivars to infections caused by *Xylella fastidiosa* subsp. *pauca*, ST53. In: *Proceedings of the 2nd European conference on Xylella fastidiosa: how research can support solutions*. Ajaccio, France, Available from: https://doi.org/10.5281/zenodo.3564485.

Saponari, M., Giampetruzzi, A., Loconsole, G., Boscia, D. & Saldarelli, P. (2019) *Xylella fastidiosa* in olive in Apulia: where we stand. *Phytopathology*, 109, 175–186.

Schneider, K., Van Der Werf, W., Cendoya, M., Mourits, M., Navas-Cortés, J.A., Vicent, A. et al. (2020) Impact of *Xylella fastidiosa* subspecies *pauca* in European olives. *Proceedings of the National Academy of Sciences of the United States of America*, 117, 9250–9259.

Sperry, J.S., Hacke, U.G. & Wheeler, J.K. (2005) Comparative analysis of end wall resistivity in xylem conduits. *Plant, Cell & Environment*, 28, 456–465.

Sun, Q., Greve, L.C. & Labavitch, J.M. (2011) Polysaccharide compositions of intervessel pit membranes contribute to Pierce's disease resistance of grapevines. *Plant Physiology*, 155, 1976–1987.

Sun, Q., Rost, T.L. & Matthews, M.A. (2006) Pruning-induced tylose development in stems of current-year shoots of *Vitis vinifera* (Vitaceae). *American Journal of Botany*, 93, 1567–1576.

Virtanen, P., Gommers, R., Oliphant, T.E., Haberland, M., Reddy, T., Cournapeau, D. et al. (2020) SciPy 1.0: fundamental algorithms for scientific computing in python. *Nature Methods*, 17, 261–272.

Walker, N., White, S., McKay Fletcher, D., Ruiz, S.A., Rankin, K.E., De Stradis, A. et al. (2022) The impact of xylem geometry on olive cultivar resistance to *Xylella fastidiosa*: an image-based study. *Plant Pathology*, 72, 521–535.

Wells, J.M., Raju, B.C., Hung, H.-Y., Weisburg, W.G., Mandelco-Paul, L. & Brenner, D.J. (1987) *Xylella fastidiosa* gen. nov., sp. nov: gram-negative, xylem-limited, fastidious plant bacteria related to *Xanthomonas* spp. *International Journal of Systematic and Evolutionary Microbiology*, 37, 136–143.

Zimmermann, M.H. (2013) *Xylem structure and the ascent of sap*, 2nd edition. Heidelberg: Springer Science & Business Media.

SUPPORTING INFORMATION

Additional supporting information can be found online in the Supporting Information section at the end of this article.

How to cite this article: Walker, N.C., Ruiz, S.A., Ferreira, T.R., Coletta-Filho, H.D., Le Houx, J., McKay Fletcher, D. et al. (2023) A high-throughput analysis of high-resolution X-ray CT images of stems of olive and citrus plants resistant and susceptible to *Xylella fastidiosa*. *Plant Pathology*, 00, 1–14. Available from: https://doi.org/10.1111/ppa.13835